Clinical Kidney Journal, 2024, vol. 17, no. 2, sfae019

https://doi.org/10.1093/ckj/sfae019
Advance Access Publication Date: 2 February 2024
Original Article

ORIGINAL ARTICLE

Recognition of intraglomerular histological features with deep learning in protocol transplant biopsies and their association with kidney function and prognosis

Imane Farhat[1,*], Elise Maréchal[1,*], Doris Calmo[2], Manon Ansart[3], Michel Paindavoine[3], Patrick Bard[3], Georges Tarris[4], Didier Ducloux[2,5], Sophie Adrian Felix[6], Laurent Martin[4], Claire Tinel[1,5], Jean-Baptiste Gibier[7], Mathilde Funes de la Vega[4], Jean-Michel Rebibou[1,5], Jamal Bamoulid[2,5] and Mathieu Legendre[1,3,5,*]

[1]Department of Nephrology, CHU Dijon, Dijon, France, [2]Department of Nephrology, CHU Besançon, Besançon, France, [3]LEAD-CNRS, UMR 5022, Université de Bourgogne, Dijon, France, [4]Department of Pathology, CHU Dijon, Dijon, France, [5]Etablissement Français du sang, Besançon, France, [6]Department of Pathology, CHU Besançon, Besançon 25000, France and [7]Department of Pathology, CHU Lille, Lille, France

*These authors contributed equally to this work as first and last authors.
Correspondence to: Mathieu Legendre; E-mail: mathieu.legendre@chu-dijon.fr

ABSTRACT

Background. The Banff Classification may not adequately address protocol transplant biopsies categorized as normal in patients experiencing unexplained graft function deterioration. This study seeks to employ convolutional neural networks to automate the segmentation of glomerular cells and capillaries and assess their correlation with transplant function.

Methods. A total of 215 patients were categorized into three groups. In the Training cohort, glomerular cells and capillaries from 37 patients were manually annotated to train the networks. The Test cohort (24 patients) compared manual annotations vs automated predictions, while the Application cohort (154 protocol transplant biopsies) examined predicted factors in relation to kidney function and prognosis.

Results. In the Test cohort, the networks recognized histological structures with Precision, Recall, F-score and Intersection Over Union exceeding 0.92, 0.85, 0.89 and 0.74, respectively. Univariate analysis revealed associations between the estimated glomerular filtration rate (eGFR) at biopsy and relative endothelial area ($r = 0.19$, $P = .027$), endothelial cell density ($r = 0.20$, $P = .017$), mean parietal epithelial cell area ($r = –0.38$, $P < .001$), parietal epithelial cell density ($r = 0.29$, $P < .001$) and mesangial cell density ($r = 0.22$, $P = .010$). Multivariate analysis retained only endothelial cell density as associated with eGFR (Beta = 0.13, $P = .040$). Endothelial cell density ($r = –0.22$, $P = .010$) and mean podocyte area ($r = 0.21$, $P = .016$) were linked to proteinuria at biopsy. Over 44 ± 29 months, 25 patients (16%) reached the primary composite endpoint (dialysis initiation, or 30% eGFR sustained decline), with relative endothelial area, mean endothelial cell area and parietal epithelial cell density below medians linked to this endpoint [hazard ratios, respectively, of 2.63 ($P = .048$), 2.60 ($P = .039$) and 3.23 ($P = .019$)].

Conclusion. This study automated the measurement of intraglomerular cells and capillaries. Our results suggest that the precise segmentation of endothelial and epithelial cells may serve as a potential future marker for the risk of graft loss.

Received: 31.10.2023; Editorial decision: 15.12.2023

GRAPHICAL ABSTRACT

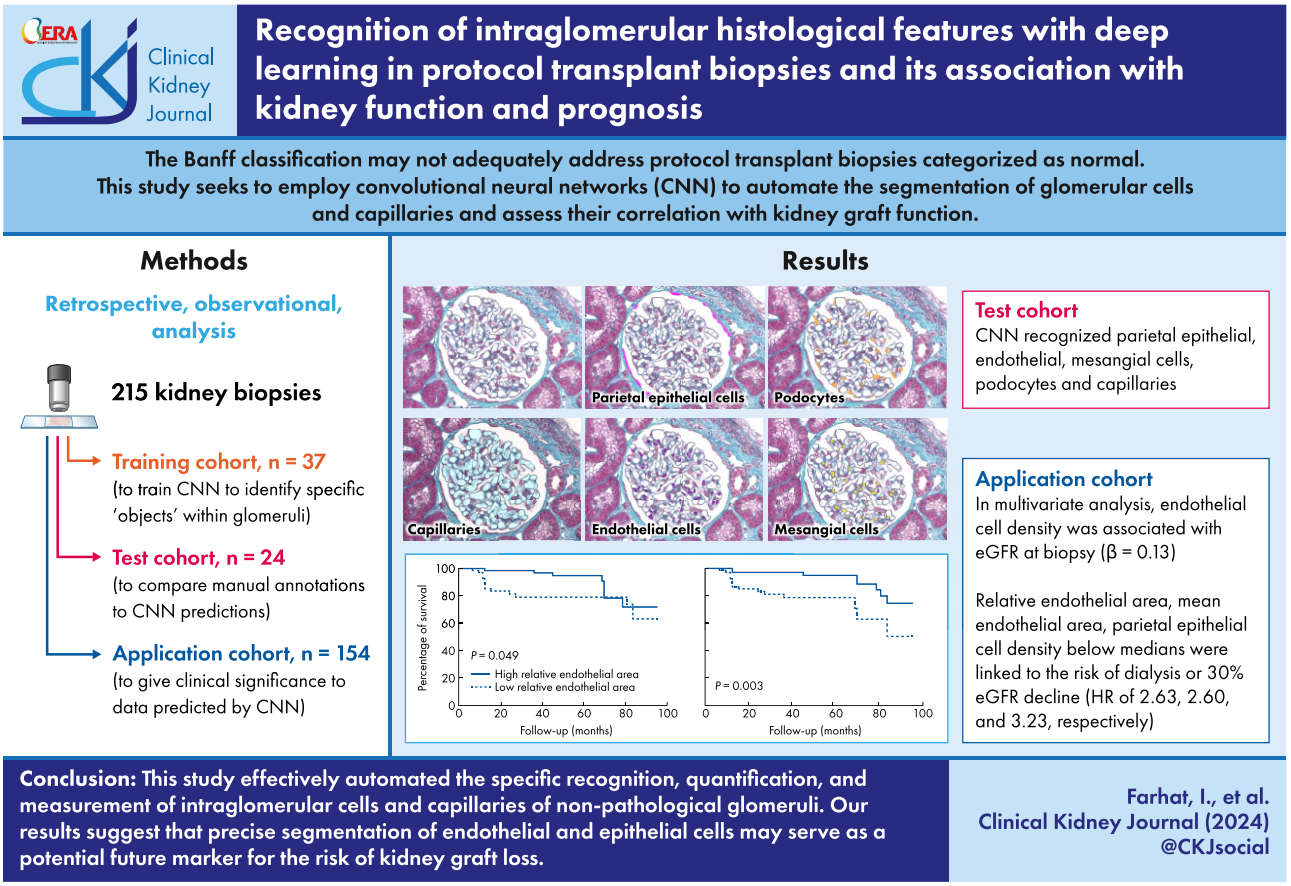

Keywords: artificial intelligence, deep learning, glomerulus, kidney pathology, transplant biopsies

KEY LEARNING POINTS

What was known:

- The Banff Classification has limitations in explaining the impairment of transplant function and the prognosis of biopsies without rejection or viral nephropathy.
- Glomerular volume and ischemia in protocol biopsies appear to be correlated with the decline in glomerular filtration rate (GFR) post-transplantation.
- No study has precisely assessed the association between glomerular cells and glomerular capillaries in protocol transplant biopsies and their impact on kidney function and prognosis.

This study adds:

- We have developed automated recognition through deep learning for parietal epithelial cells, podocytes, mesangial cells, endothelial cells and glomerular capillaries of non-pathological glomeruli.
- Several new histological markers have been evaluated, demonstrating the statistical association between endothelial cell density and estimated GFR (eGFR), confirming the association between podocyte area and proteinuria, and suggesting a potential link between a decrease in relative glomerular capillary area and initial graft dysfunction.
- We have shown that low mean and relative endothelial areas, as well as low epithelial cell density, may be associated with higher risks of graft function deterioration.

Potential impact:

- These five freely available algorithms could assist pathologists in automating the assessment of various new specific markers for kidney transplant prognosis of non-pathological glomeruli.
- This work could lead to studies targeting the endothelial and parietal cell populations in transplantation.
- The observed correlations between glomerular cellular populations and eGFR could allow for the adjustment of nephroprotective treatments based on protocol biopsy assessments or facilitate tailored therapies for these specific cells in the future.

INTRODUCTION

Protocol graft biopsies play a pivotal role in monitoring transplanted patients. These biopsies are essential for detecting toxicity from calcineurin inhibitors, recurrences of kidney diseases, viral nephropathies and particularly rejection episodes. In most cases, the presence of lesions prompts specific treatment administration and/or adjustments to the maintenance immunosuppressive regimen, all aimed at improving graft survival [1–6].

Histological abnormalities in kidney transplantation are primarily categorized within the International Banff Classification [7]. This classification has limitations when it comes to cases without rejection, viral nephropathy, or drug toxicity. Thus, the Banff Classification appears inadequate for biopsies categorized as normal in patients experiencing unexplained graft function deterioration [8].

Recent studies have explored the association between glomerular anatomy, which is not extensively described in the Banff Classification, and its impact on kidney function [9]. Denic *et al.* observed an association between glomerular volume, ischemic glomeruli and the risk of graft loss [10]. To our knowledge, no study has comprehensively investigated the association between glomerular cells or capillaries and transplant function.

Manually conducting an exhaustive exploration of intrinsic glomerular elements across entire cohorts is virtually impossible. Such a task would require the segmentation of several hundred thousand elements. Artificial intelligence may offer a solution to these challenges [11]. Our team and others have demonstrated that convolutional neural networks (CNNs) can be a valuable tool for analyzing glomerular architecture in conditions such as minimal change disease (MCD), lupus nephritis, immunoglobulin A nephropathy and diabetes [12–16]. However, these studies have primarily focused on lesions and/or were not trained to simultaneously detect all glomerular cells and capillaries.

This study aims to automate the segmentation of most intrinsic glomerular elements using CNNs on "normal" protocol kidney biopsies and subsequently evaluate the correlation between these parameters and transplant function.

MATERIALS AND METHODS

Study population

Included patients met the following criteria:

- Underwent protocol transplant biopsies from deceased donors conducted between 3 and 6 months post-kidney transplantation at the Besançon University Hospital between January 2012 and 2021, or at Dijon University Hospital between January 2020 and 2022.
- Underwent native kidney biopsies at Dijon between January 2010 and 2021 with a diagnosis of MCD.

All consenting patients (>18 years old) were evaluated for inclusion, except 6 randomly selected MCD, as 40 MCD appeared sufficient for annotation. MCD had at least 7 analyzable glomeruli, but transplant biopsies with <7 glomeruli were not excluded (included in Training or Test cohorts). Biopsies with a prior diagnosis of acute/chronic T-cell/antibody-mediated rejection (2019 Banff Classification) were excluded [17]. The remaining biopsies underwent analysis with all available stains to confirm the absence of rejection, exclude blurred or altered trichrome, and grade the Banff Classification [17]. Additional exclusions encompassed recurrent initial nephropathies, *de novo* glomerulopathies, viral nephropathies, chronic hepatitis and HIV infections.

Retrospective collection of clinical and biological characteristics from patients' records included age, gender, body mass index (BMI), diabetes, hypertension, serum creatinine levels, donor-specific antibodies positivity, BK polyomavirus replication in blood and proteinuria. Transplant-related data included

occurrence of delayed graft function, as well as immunosuppressive regimens [18].

Donor characteristics were also recorded, comprising age, gender, BMI, history of diabetes, hypertension, serum creatinine levels and proteinuria at the time of donation.

The estimated glomerular filtration rate (eGFR) was calculated using the Chronic Kidney Disease Epidemiology Collaboration formula [19].

Follow-up for transplanted patients extended from the date of transplantation to death, graft loss or the last nephrology consultation. The primary composite endpoint was defined as dialysis initiation, or a $\geq$30% sustained decrease in eGFR from biopsy (persisting for at least three consecutive months and until the last follow-up). Rejection diagnosis during follow-up depended on medical records, required a biopsy and had to adhere to the 2019 Banff criteria [17]. The follow-up period concluded in January 2021.

The retrospective study protocol was in accordance with the institutional ethic committee and with the Helsinki Declaration of 1975, as revised in 2013, and with the Principles of the Declaration of Istanbul. All patients had given oral consent for research use prior to the biopsy.

Training, Test and Application cohorts

The Training cohort was designed to train CNNs to identify specific "objects" within glomeruli. These objects included parietal epithelial, endothelial, mesangial cells, podocytes and capillaries. The number of biopsies was arbitrarily defined to train at least 500 objects per category. To facilitate future algorithm generalization, native kidney biopsies with MCD were incorporated into both the Training and Test sets. The Training cohort comprised 37 biopsies from Dijon, including 11 protocol transplant biopsies and 26 MCD.

The Test cohort was designed to compare manual annotations with CNNs' predictions to validate detection performance. No Test group patients were included in the Training group. MCD biopsies were distributed with a 2/3 ratio in the Training cohort and 1/3 in the Test cohort. All transplant biopsies from Besancon with $<$7 glomeruli were included in the Test cohort, as it did not require correlation with clinical data and a single glomerulus sufficed. This group consisted of 10 protocol transplant biopsies from Besançon and 14 MCD biopsies from Dijon.

The Application cohort aimed to give clinical significance to the numerical data extracted from predictions by CNNs. This cohort comprised 154 protocol transplant biopsies from Besançon, each containing $>$7 glomeruli.

Histological analysis

Kidney biopsies from formalin-fixed, paraffin-embedded tissues were sectioned into 2 μm sections and stained with Masson's trichrome, periodic acid–Schiff and Jones stains. Immunofluorescence data (including C4d) were extracted from the pathology report. No electron microscopy analysis was performed. The blind examination and annotation of biopsies were conducted, with glomeruli pre-annotated by a junior pathologist. Two kidney pathologists (holding a French diploma in kidney pathology) collectively corrected annotations through consensus.

Whole-slide images pre-processing

Biopsies were digitized using a Hamamatsu scanner (model C9600-12) with a 20$\times$ lens (NDPI format). Images were then transformed into JPEG format at a fixed resolution of 450 nm/pixel. Glomeruli were analyzed at 40$\times$ magnification. Manual annotations were performed using ASAP annotation software (version 1.9). Training and testing required separate manual annotations of objects: the capillaries (encompassing endothelial cells) and the cytoplasm of the different cells.

In the Application cohort, all analyzable glomeruli were used. Only the outer part of the Bowman's capsule was manually annotated (40$\times$ zoom). In the Training and Test groups, annotating all glomeruli manually would have been practically unfeasible due to the large number of objects, as each glomerulus required annotation for all its cells and capillaries. Thus, cortical areas in these groups were divided into 3840 $\times$ 2176 pixel rectangles (20$\times$ zoom) containing glomeruli (Supplementary data, Fig. S1). A random rectangle was chosen, and a new capture of each glomerulus at 40$\times$ zoom (1920 $\times$ 1088 pixels) was taken. A program identified and extracted glomerulus annotations, automatically centering each in a vignette of 1024 $\times$ 1024 pixels. One to three randomly selected glomeruli per patient were analyzed. Fifty-two glomeruli were used for training, and 29 for testing.

Algorithms

Training and evaluations were conducted using a computer equipped with the Titan RTX 133 (Nvidia, CA, USA) graphics card (24 GB VRAM). We used the Mask R-CNN Inception ResNet V2 (faster_rcnn_inception_resnet_v2_keras) CNN, and the implementation was carried out in Python using Tensorflow and Keras [12, 13, 20]. Adopting a glomerular training methodology akin to our prior work, we made minimal hyperparameter adjustments, setting warm-up steps to 50 and a learning rate of 0.008 [13]. The Mask-RCNN was pretrained using the "TF2 Detection Zoo" version (https://github.com/tensorflow/models/blob/master/research/object_detection/g3doc/tf2_detection_zoo.md). Data augmentation, to artificially augment the training data, involved random 90° rotations for each image at each epoch (a complete cycle of CNN training).

The Training cohort images dataset was split into an 80%/20% ratio at the patient level for training and validation, and converted into TFrecords. At each epoch, the algorithm adjusted based on agreement between predictions and manual annotations of the validation dataset. The number of epochs for each training was visually determined by continuously analyzing the learning curves in Tensorboard, and manual intervention stopped training when an asymptote was apparent. Initial training attempts using all categories of annotations yielded unsatisfactory predictions. Consequently, each object underwent separate training. The training process for all glomerular cells and capillaries required 150 epochs, except endothelial cells which required 100 epochs. A total of 879 parietal epithelial cells, 1170 podocytes, 2071 mesangial cells, 2091 endothelial cells and 3359 glomerular capillaries were annotated.

Predicted data

The glomerular data utilized in the Application cohort included objects' area and count. These data facilitated the extrapolation of the mean area of objects, the mean total objects' area per glomerulus, the ratio between objects and glomerular areas (referred to as relative area) and object density per glomerular area. As capillaries do not have a spherical shape in space, density measurements were exclusively used for cells and were extrapolated from the glomerular density formula

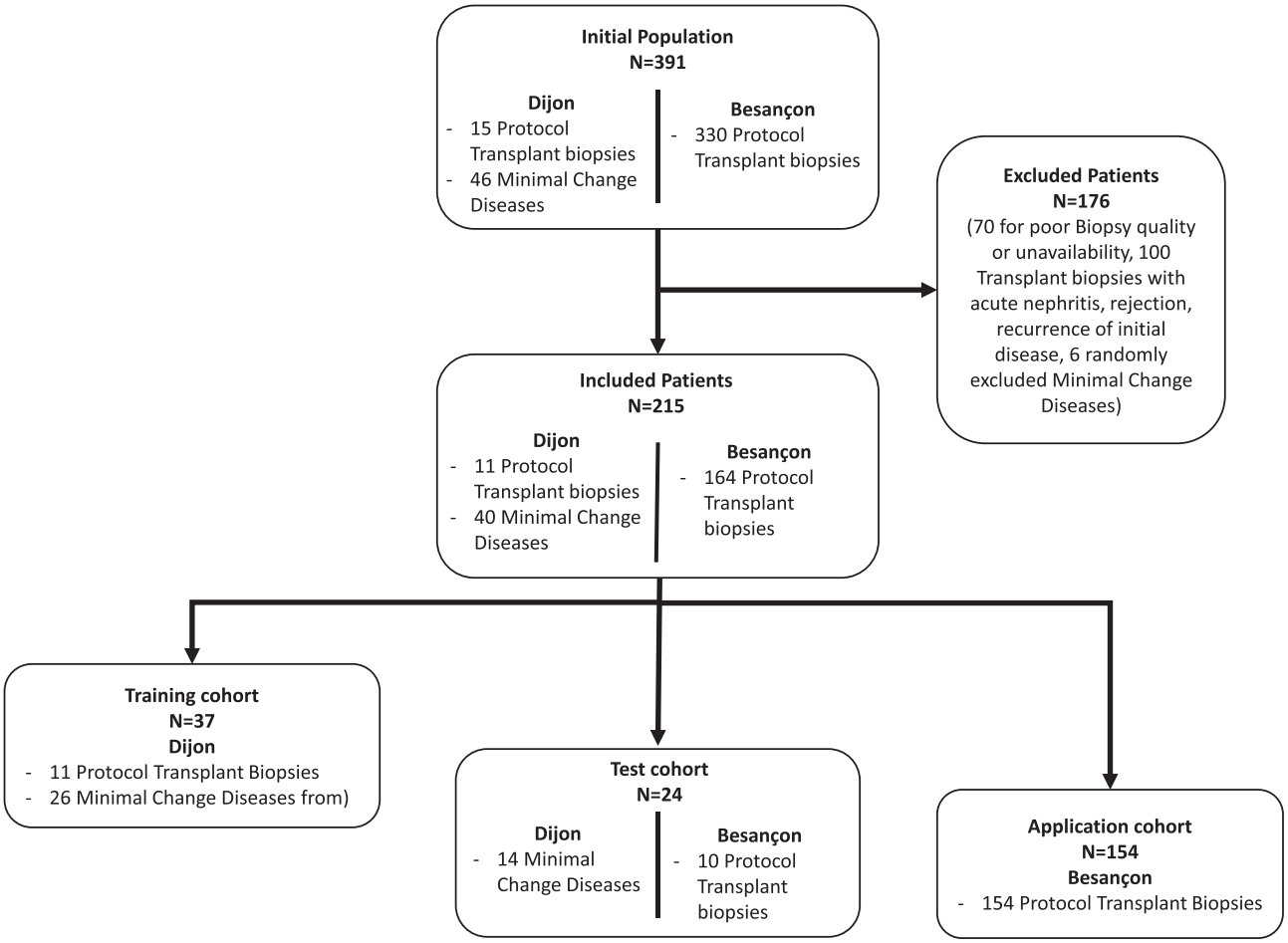

Figure 1: Flow chart.

[9]. The formulas and extended methods are described in the Supplemental Materials and Supplementary data, Table S1.

Statistical analyses

Quantitative and categorical data were respectively expressed as means ± standard deviations and *n* (%). The correlation between two variables was assessed using the Spearman test. To examine the association between eGFR and other variables, a backward multiple linear regression test was conducted, after excluding variables with collinearity (Variance inflation factor >4), including significant data from univariate tests. Mann–Whitney's test was used to compare two quantitative variables.

The performance of the CNNs was evaluated using Precision, Recall, F-score and Intersection Over Union (IOU) (Supplementary data, Table S1) [12].

The risk of the primary endpoint was assessed using the Log-Rank survival test for univariate analysis and the Cox model for multivariate analysis. Criteria determined through the Log-Rank test with $P < .1$ were included in the Cox model. A significance level of <5% was considered statistically significant. Analyses were conducted using GraphPad PRISM 6.01 (GraphPad Software, La Jolla, CA, USA) and IBM SPSS 23 softwares (IBM, Chicago, IL, USA).

RESULTS

Populations

A total of 215 patients were included, divided into three groups (Fig. 1). The mean age at biopsy was 54 ± 17 years, with 131 patients (61%) being male. Mean creatinine, eGFR and proteinuria at biopsy were 1.4 ± 0.5 mg/dL, 59±25 mL/min/1.73 m^2 and 1.8 ± 4.5 g/day, respectively. Due to the inclusion of MCD, patients in the Training and Test cohorts tended to be younger and to have higher eGFR and proteinuria (Table 1).

Detection accuracy

In the Test cohort, 24 glomeruli were randomly selected to compare CNNs' predictions with manual annotations. The CNNs demonstrated reliable recognition of histological structures, with Precision, Recall, F-score and IOU all exceeding 0.92, 0.85, 0.89 and 0.74, respectively (Fig. 2, Table 2). An analysis focusing solely on transplant biopsies yielded similar results (Supplementary data, Table S2). Mesangial cells and podocytes exhibited the weakest detection capabilities. Other common errors included: undetected endothelial cells, confusion between podocytes and epithelial/endothelial cells, failure to recognize some capillaries or boundary delineation issues.

Table 1: Population characteristics.

Data	Population total (N = 215)	Training cohort (N = 37)	Test cohort (N = 24)	Application cohort (N = 154)
Age (years)	54 ± 17	49 ± 17	46 ± 17	55 ± 13
Male sex	131 (61)	18 (49)	17 (71)	96 (62)
Hypertension	168 (78)	13 (35)	15 (63)	140 (93)
Diabetes	42 (20)	6 (16)	2 (8)	34 (22)
Transplant	175 (81)	11 (30)	10 (42)	154 (100)
MCD	40 (19)	26 (70)	14 (58)	0 (0)
Serum creatinine level at biopsy (mg/dL)	1.4 ± 0.5	1.1 ± 0.4	1.3 ± 0.5	1.5 ± 0.5
eGFR at biopsy (mL/min/1.73 m^2)	59 ± 25	75 ± 27	73 ± 31	53 ± 20
Proteinuria at biopsy (g/day)	1.8 ± 4.5	4.7 ± 5.8	6.5 ± 9.2	0.3 ± 0.3

Quantitative data are expressed as means ± standard deviations, semi-quantitative data are expressed as numbers (percentages).

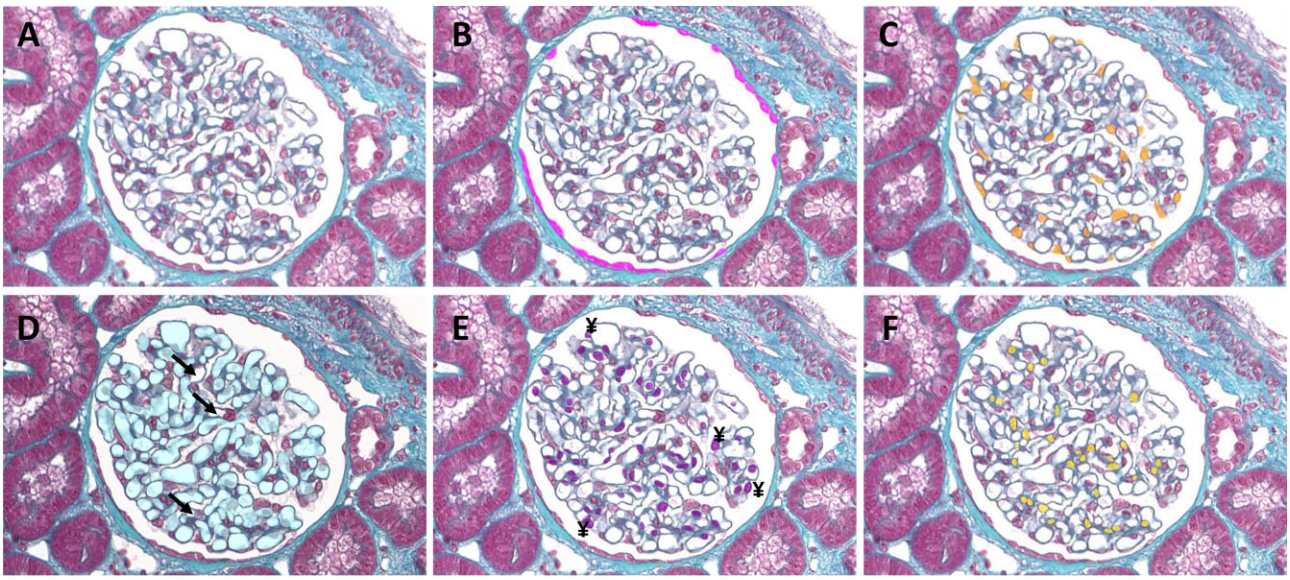

Figure 2: Predictions of CNNs within the glomerulus of a transplanted patient included in the Test cohort. (**A–F**) Glomerulus stained with Masson's trichrome (×40 zoom). Parietal epithelial cells, podocytes, capillaries endothelial cells and mesangial cells were artificially colored respectively in pink (B), orange (C), light blue (D), purple (E) and yellow (F). Arrows: capillaries not detected by convolutional neural network; ¥: podocyte detected as endothelial cells.

Table 2: Convolutional neural networks accuracy in the Test cohort.

Objects	Number of objects	Precision[a]	Recall[b]	F-score[c]	IOU[d]
Parietal epithelial cells	539	0.96	0.89	0.92	0.82
Podocytes	633	0.93	0.86	0.89	0.75
Mesangial cells	907	0.93	0.88	0.90	0.74
Endothelial cells	1576	0.93	0.93	0.93	0.79
Capillaries	2029	0.99	0.94	0.96	0.93

[a]Precision: percentage of items belonging to the interest class among items identified as belonging to the interest class.
[b]Recall: percentage of items identified as belonging to the interest class among all items belonging to the interest class.
[c]F-score: 2*(Precision*Recall)/(Precision + Recall)
[d]IOU: (common area between the predicted and the annotated object)/(area of the predicted object 1 area of the annotated object – common area of the annotated and predicted object).

Association between predictions and kidney function

Among the 154 patients in the Application cohort, the mean age at biopsy was 55 ± 13 years, with 96 patients (62%) being male. Mean serum creatinine level, eGFR and proteinuria at biopsy were 1.5 ± 0.5 mg/dL, 53±20 mL/min/1.73 m^2 and 0.3 ± 0.3 g/day, respectively (Table 1). Thirty patients (19%) have had at least one dosage of BK polyomavirus replication in their blood, and five patients (3%) had donor-specific antibodies before the biopsy. Immunosuppressive regimens were relatively homogenous between patients. Extended recipients' and donors' data are described in Supplementary data, Table S3.

Table 3: Histological analyses of protocol biopsies.

Data	Application cohort (*N* = 154)
Number of glomeruli	23 ± 12
Banff score[a]	
g score ≥1	3 (2)
mm score ≥1	37 (24)
cg score ≥1	1 (1)
i score ≥1	3 (2)
t score ≥1	2 (1)
ptc score ≥1	2 (1)
ah score ≥1	79 (51)
cv score ≥1	52 (34)
v score ≥1	0 (0)
IF/TA score	
1	68 (44)
2	4 (3)
3	1 (1)
Predicted data	
Number of parietal epithelial cells per glomerulus	16 ± 4
Relative parietal epithelial area (%)	2.5 ± 0.7
Mean parietal epithelial cell area (μm^2)	33 ± 3
Parietal epithelial cell density (cell/mm^2)	6503 ± 1842
Number of podocytes per glomerulus	22 ± 5
Mean podocyte area (μm^2)	790 ± 192
Relative podocyte area (%)	3.5 ± 0.6
Podocyte density (cell/mm^2)	8668 ± 2452
Number of endothelial cells per glomerulus	29 ± 13
Mean endothelial cell area (μm^2)	18 ± 1
Relative endothelial area (%)	2.3 ± 0.9
Endothelial cell density (cell/mm^2)	14 998 ± 6025
Number of mesangial cells per glomerulus	28 ± 10
Mean mesangial cell area (μm^2)	553 ± 194
Relative mesangial area (%)	2.5 ± 0.6
Mesangial cell density (cell/mm^2)	14 267 ± 3719
Number of capillaries per glomerulus	64 ± 14
Mean capillary area (μm^2)	102 ± 15
Relative capillary area (%)	29.0 ± 3.6

Quantitative data are expressed as means ± standard deviations, semi-quantitative data are expressed as numbers (percentages).
[a]Banff score elements as previously published [7].

The biopsies included a mean of 23 ± 11 glomeruli. None of the biopsies met the histological criteria for rejection, viral nephropathy or recurrence of the initial disease. Banff scores as well as histological predicted data are provided in Table 3. The mean inference time of CNNs was 5 min per biopsy. Within the 3514 analyzed glomeruli, 57 323 parietal epithelial cells, 78 905 podocytes, 100 171 endothelial cells, 99 366 mesangial cells and 223 574 glomerular capillaries were detected.

In univariate analysis, factors associated with eGFR at biopsy included relative endothelial area (r = 0.19, *P* = .027), endothelial cell density (r = 0.20, *P* = .017), mean parietal epithelial cell area (r = –0.38, *P* < .001), parietal epithelial cell density (r = 0.29, *P* < .001), relative mesangial area (r = 0.18, *P* = .030) and mesangial cell density (r = 0.22, *P* = .010) (Fig. 3). Relative capillary area did not reach significance (r = 0.16, *P* = .055). Other factors associated with eGFR were donor and recipient age, BMI, histories of diabetes, donor sex, hypertension and histologic scores of interstitial fibrosis/tubular (IF/TA) atrophy and vascular fibrous intimal thickening (cv). As relative areas and densities, as well as the age of the donor and recipient, were considered covariates, both relative areas and the recipient's age were excluded from the multivariate analysis. In multiple linear regression, the only factors that remained associated with eGFR were endothelial cell density [Beta = 0.13, 95% confidence interval (CI) 0.06–0.32, *P* = .040) and donor age (Beta = –0.68, 95% CI –0.80 to –0.56, *P* < .001) (Supplementary data, Table S4).

Histological factors associated with proteinuria at biopsy included endothelial cell density (r = –0.22, *P* = .010) and mean podocyte area (r = 0.21, *P* = .016). The mean podocyte areas were significantly larger in the MCD biopsies (Test cohort) compared with those from transplanted patients (Application cohort) (*P* < .001) (Supplementary data, Fig. S2).

Relative capillary area correlated with initial hospitalization duration (r = –0.17, *P* = .040) and eGFR at discharge (r = 0.24, *P* = .004). Although not significant, patients with delayed graft function (*n* = 16) tended to have a smaller relative capillary area (*P* = .09).

Predicted parameters were mainly correlated with donor characteristics such as gender, age and BMI. The correlated data are described in Supplementary data, Table S5. While relative capillary area was negatively correlated (r = –0.31, *P* < .001), mesangial cell density was positively correlated (r = 0.21, *P* < .009) with matrix expansion score (mm). Patients with an mm score ≥1 had lower relative capillary areas, and higher mesangial cells densities and relative areas (Supplementary data, Fig. S3).

Follow-up

During a mean follow-up of 44 ± 29 months, 10 patients (6%) died (6 of unknown causes, 2 of vascular causes, 1 of cancer, 1 of suicide), 6 (4%) experienced acute rejections (3 T-cell-mediated, 3 antibody-mediated), 6 (4%) lost their transplants (2 chronic mixed rejections, 2 BK polyomavirus infections, 1 progressive decline and 1 recurrence of membranoproliferative glomerulonephritis) and 25 (16%) reached the primary composite endpoint (initiation of dialysis, or a 30% decline in eGFR).

Visual assessment revealed challenges in distinguishing biopsies with low versus high endothelial relative and mean areas. However, in univariate analysis, having relative and mean endothelial areas below the medians were associated with the occurrence of the primary composite endpoint [hazard ratios (HRs) of 2.24, 95% CI 1.03–5.12, *P* = .049, and 3.20, 95% CI 1.58–8.17, *P* = .003] (Fig. 4). The associations of parietal epithelial cell density and mean podocyte area with the composite endpoint did not reach significance. Hypertension, diabetes, BMI, donor-specific antibodies and BK polyomavirus replication at biopsy also tended to be associated with the prognosis (Table 4). In multivariate analysis, low relative endothelial area, mean endothelial area and parietal epithelial cell density were associated with the composite endpoint (HRs, respectively, of 2.63, 95% CI 1.01–6.84, *P* = .048, and 2.60, 95% CI 1.05–6.44, *P* = .039, and 3.23, 95% CI 1.21–8.60, *P* = .019). Recipient history of diabetes, and BK polyomavirus replication were also linked to the endpoint (Table 4).

The mean time to rejection was 18 ± 16 months. Among seven patients with rejection, three (two acute antibody-mediated and one chronic mix) achieved the primary composite endpoint. Only one patient (acute T-cell-mediated rejection) among the seven had a relative endothelial area above the median. In univariate survival analyses of histological markers, only a relative endothelial area below the median was associated with an elevated rejection risk (HR 8.62, 95% CI 1.51–30.76, *P* = .014) (Supplementary data, Fig. S4).

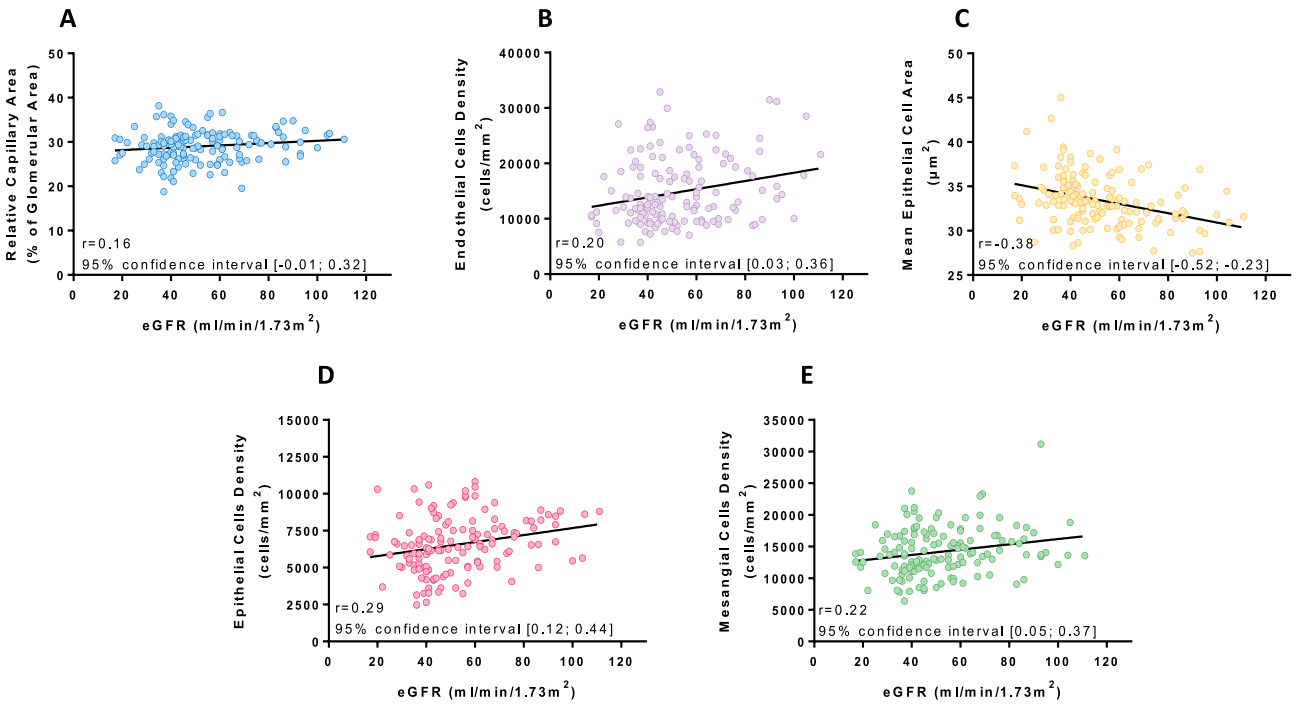

Figure 3: Associations between CNNs' predictions and eGFR at biopsy in the Application cohort. The significant correlations between eGFR and factors predicted by the convolutional neural networks were assessed by Spearman correlation test.

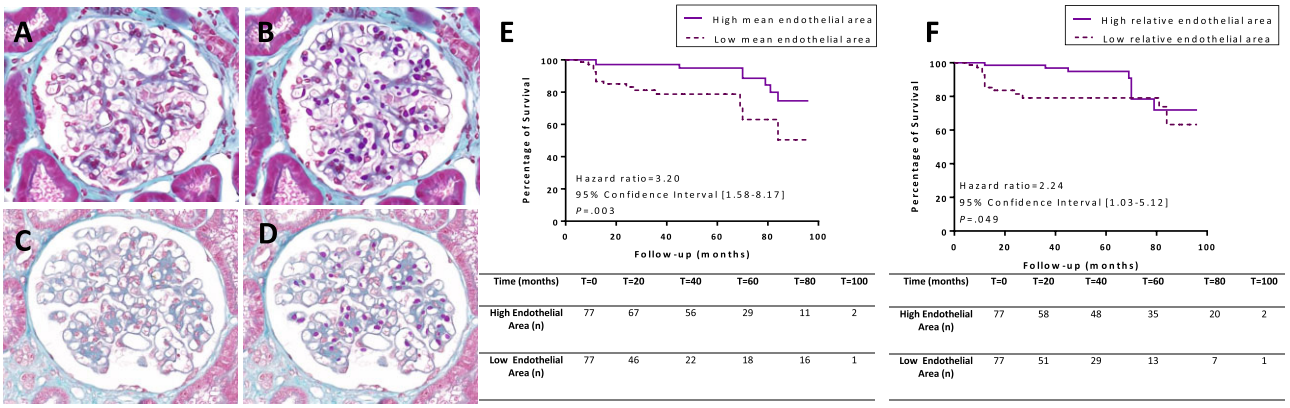

Figure 4: Relation between mean and relative endothelial areas and kidney prognosis. Example of protocol transplant biopsies (**A–D**) without significant interstitial fibrosis, inflammation or intimal fibrosis (×40 zoom) stained with Masson's trichrome before (A, C) and after (B, D) CNN detection of endothelial cells. Endothelial cells were artificially colored by the network in purple. (A, B) Biopsy of a patient with a high mean (19 µm²) and relative endothelial (5.2%) areas who did not reach the primary endpoint (initiation of dialysis, or a 30% decline in GFR from biopsy). (C, D) Biopsy of a patient with a low mean (16 µm²) and relative endothelial (1.1%) areas who reach the primary endpoint. (**E, F**) Kaplan–Meier curves of survival analysis and number at risk tables of the primary composite endpoint depending on whether mean and relative endothelial areas were above or under the medians.

DISCUSSION

In this study, we fully automated the analysis of all cells and capillaries populating the non-pathological glomeruli and investigated their relationship with transplant function. These predictions, particularly those related to endothelial cells, exhibited associations with eGFR, proteinuria and transplant prognosis.

Our tool enabled an inexpensive and rapid analysis of intrinsic glomerular parameters with a strong correlation between predicted and observed structures. The highest accuracy was achieved in detecting capillaries, while mesangial cells and podocytes exhibited lower performance. Limitations in our training included the restricted number of annotated glomeruli, despite a considerable quantity of total objects. Another limitation was the lack of a comparison with immunohistochemistry for each cell type to validate our annotations. Similar to Govind *et al.*'s approach in their podocyte nucleus recognition study, sequential labeling on the same section before or after trichrome staining could have been employed [16]. Alternatively, each marker could have been established on individual sections. Additionally, our collaborative analysis for annotation precluded the assessment of variability among pathologists.

Table 4: Survival analysis of the composite criteria dialysis initiation, or 30% eGFR sustained decline.

N = 154	Univariate[a]		Multivariate[b]	
Factors	HR (95% CI)	*P*-value	HR (95% CI)	*P*-value
Recipient's data at biopsy				
Age (per year)	1.02 (0.99–1.05)	.268		
Male sex	1.26 (0.61–3.14)	.449		
Hypertension	3.31 (1.65–35.35)	**.10**		
Diabetes mellitus	5.13 (3.05–42.00)	**<.001**	2.92 (1.08–7.88)	**.035**
BMI (per kg/m^2)	1.12 (1.04–1.22)	**.004**		
BK virus replication	6.01 (7.92–90.21)	**<.001**	6.14 (2.32–16.28)	**<.001**
Donor-specific antibodies	3.67 (0.98–178.80)	.056		
eGFR (per mL/min/1.73m^2)	0.99 (0.97–1.02)	.818		
Proteinuria (per g/day)	2.17 (0.73–6.46)	.163		
Predicted histological data				
Relative parietal epithelial area[c]	1.73 (0.78–3.86)	.183		
Mean parietal epithelial cell area[c]	0.82 (0.37–1.81)	.619		
Parietal epithelial cell density[c]	2.23 (0.97–4.80)	.064	3.23 (1.21–8.60)	**.019**
Mean podocyte area[c]	2.04 (1.06–5.83)	.053	2.63 (0.91–7.61)	.074
Relative podocyte area[c]	0.69 (0.31–1.55)	.377		
Podocyte density[c]	1.25 (0.56–2.80)	.297		
Mean endothelial cell area[c]	3.20 (1.58–8.17)	**.003**	2.60 (1.05–6.44)	**.039**
Relative endothelial area[c]	2.24 (1.03–5.12)	**.049**	2.63 (1.01–6.84)	**.048**
Endothelial cell density[c]	1.72 (0.79–3.93)	.179		
Mean mesangial cell area[c]	1.49 (0.67–3.33)	.330		
Relative mesangial area[c]	1.04 (0.47–2.33)	.925		
Mesangial cell density[c]	1.82 (0.84–4.24)	.131		
Mean capillary area[c]	0.89 (0.40–1.96)	.762		
Relative capillary area[c]	1.05 (0.47–2.35)	.908		
Banff score[d]				
t score ≥1	2.15 (0.18–56.36)	.435		
ptc score ≥1	0.35 (0.02–5.62)	.457		
g score ≥1	1.61 (0.15–22.43)	.635		
mm score ≥1	0.84 (0.33–2.17)	.731		
cg score ≥1	4.34 (0.50–15.85)	.111		
i score ≥1	1.74 (0.16–28.15)	.579		
ah score ≥1	1.02 (0.46–2.27)	.966		
IF/TA score ≥1	1.72 (0.79–4.02)	.173		
cv score ≥1	1.27 (0.53–3.13)	.581		

[a]Log-Rank survival test or Cox survival test

[b]Cox Survival Model including hypertension, diabetes mellitus, BMI, BK polyomavirus replication, donor-specific antibodies positivity, parietal epithelial cell density, mean podocyte area, mean endothelial cell area and relative endothelial area.

[c]Under versus above the median.

[d]Banff score elements as previously published [7].

P-values of the factors statistically associated with the endpoint occurrence are in bold type.

We used the same CNN as in our previous works which is suited for the segmentation of small-sized elements like glomerular cells [12, 13, 20]. Even if Masson's trichrome allows the recognition of glomerular elements, most of glomerular studies are performed with periodic acid–Schiff [21–23]. We chose Masson's trichrome as our previous algorithms targeting glomeruli were only trained and evaluated with this stain. The strong association observed between glomerular predictions and donor characteristics reinforces the credibility of the CNN's predictions. From our perspective, including native kidneys biopsies in the training dataset did not introduce a significant bias as discerning a MCD glomerulus from a transplant glomerulus appeared nearly impossible. Additionally, the training included transplant biopsies, and predictions on normal transplant biopsies in the Test cohort appeared as robust as those on MCD. The inclusion of native kidney biopsies may enable pathologists to utilize these algorithms for other indications.

Decreased endothelial cell density, relative area and mean area were linked to kidney function, proteinuria and the occurrence of the composite endpoint. Glomerular endothelial cells, lining capillary lumens with fenestrated endothelium, play a pivotal role in various pathologies. They secrete nitric oxide, exhibiting anti-inflammatory and vasodilatory properties. Damage can induce a pro-inflammatory and vasoconstrictive phenotype [24]. Chronic kidney disease is often linked to markers of endothelial dysfunction and apoptosis [25, 26]. Kidney transplant factors, such as ischemia–reperfusion injuries, rejection episodes and calcineurin inhibitors, contribute to endothelial injury [27, 28]. This dysfunction leads to microvascular rarefaction and increased fibrosis, both associated with chronic graft dysfunction [24]. A low relative endothelial area was associated with a higher risk of rejection. The occurrence of the primary endpoint may in part result from this heightened susceptibility. Endothelial cells are a central target for the host immune system and can activate T cells [29]. Sis *et al.* showed that

increased expression of endothelial transcripts predicts antibody-mediated allograft lesions and poor graft outcomes [30]. The relative endothelial area might correlate with the T-cell activation profile of these cells, and its decrease could be an early indicator of rejection. Our results should be interpreted with caution as all type of rejections were collectively analyzed and were infrequent, and only three out of seven patients with rejection met the primary outcome. We also could not determine whether endothelial depletion and reduced volume caused kidney function loss or were a consequence. Regarding proteinuria, studies have suggested that glomerular endothelial cell injuries contribute to albuminuria onset in animal models of diabetic nephropathy [31]. The loss of their glycocalyx would lead to increased permeability and albuminuria [32]. Mitochondrial damage of these cells would also precede podocyte damage, and proteinuria [31, 33].

Kidney function decline correlated with parietal epithelial cell density. Glomerular parietal epithelial cells, forming the parietal layer of the urinary chamber [34, 35], help to maintain the filtration barrier by generating new podocytes [36, 37]. According to Chang *et al*., these cells can exhibit a high intracellular albumin concentration, limiting its entry into the urinary space [38]. Smeets *et al*. found that their alterations are involved in focal segmental glomerulosclerosis occurrence, contributing to the formation of synechiae [39]. These findings might explain why patients with higher parietal epithelial cell density experienced better kidney prognosis.

eGFR at biopsy correlated with mesangial cell density in univariate analysis. Mesangial cells support the glomerular tuft through the mesangial matrix, regulate the filtration barrier and help with the clearance of microparticles [40]. Under pathological stimuli, they can secrete growth factors and cytokines like transforming growth factor-β, contributing to chronic kidney disease progression. In glomerular diseases, mesangial proliferation is often associated with eGFR deterioration [41]. One could hypothesize that physiological depletion also signifies a limitation in their support quality. It should be noted that the effect of mesangial cell density was no longer significant in multivariate analysis. This univariate association may indirectly reflect correlations between endothelial and mesangial densities.

As expected, proteinuria at the time of biopsy was positively associated with mean podocyte area. Indeed, the increase in podocyte volume is one of the main lesions of diabetic nephropathy and focal segmental glomerulosclerosis [42, 43]. Podocytes lesions are responsible for disorganization of their cytoskeleton, foot process effacement, loss of slit diaphragm function and the onset of proteinuria [44]. In transplantation, transitioning from the state of having two kidneys to one graft results in kidney hypertrophy and hyperfiltration [45]. This hyperfiltration induces cytoskeletal reorganization with podocyte hypertrophy, dedifferentiation through Pax2 overexpression and reduced transcription of glomerular basement membrane adhesion genes (*nephrin*, *integrin* $\alpha 3$ and *synaptopodin*), ultimately leading to their detachment into the urinary chamber [45–48]. These phenomena promoting proteinuria and glomerulosclerosis may be exacerbated by donor–recipient size mismatches, immunosuppressive agents and the occurrence of glomerular injuries such as transplant glomerulopathy [47–50]. Monitoring the mean podocyte area could help identify patients who might benefit from early treatment with a renin–angiotensin system blocker. However, this podocyte hypertrophy associated with the alteration of the actin cytoskeleton appears to be less pronounced than that observed in MCD [51]. Indeed, in our study, podocytes from MCD had larger mean areas compared with those in transplant biopsies. While not statistically significant, the transplant podocyte area tended to be negatively associated with the risk of eGFR deterioration. These patients with higher initial proteinuria potentially received renin–angiotensin system blockers more frequently for improved nephroprotection. In contrast to our results, several studies have demonstrated that podocyte density and podocyte loss were correlated with eGFR and long-term allograft failure [45, 49, 52]. Naik *et al*. showed that this accelerated loss of podocytes preceded proteinuria and eGFR decline [53]. This phenomenon was associated with donor size, thus appearing to contrast with our findings where podocyte density showed a negative association with the donor's BMI. In our study, a lack of statistical power and the influence of other markers, such as endothelial cells, may have diminished the impact of podocyte density on transplant outcomes.

The relative capillary area correlated with hospitalization duration and eGFR at hospital discharge. Doreille *et al*. had previously reported an association between peri-tubular capillary density and delayed graft function [54]. The alignment between our results and those of Doreille *et al*. may stem from the terminal nature of kidney vascularization, with peritubular capillaries representing a continuation of glomerular capillaries. Our evaluation was conducted after the initial hospitalization, which limits its interpretation.

The predicted data seemed to accurately mirror the architecture of the donors' kidneys, often aligning with the donors' characteristics at the time of donation. Obtaining these data from protocol biopsies at 1 year or later might have increased the likelihood of correlating with recipient characteristics. Denic *et al*. found that glomerular volume and percentage of ischemic glomeruli correlated more strongly with donor data when biopsies were conducted within the first year and with recipient data when performed later [10].

Our study benefits from a relatively homogeneous population limiting bias linked to the effects of treatments variations, rejections and infections. We provide novel insights into the impact of various cellular and capillary elements within glomerular architecture, which have not been comprehensively described before. The predicted parameters demonstrated a correlation with eGFR close to that of IF/TA. However, these associations between histological features and clinical measurements were rather small. Factors such as hydration status or the dosage of calcineurin inhibitors may independently affect kidney function, limiting the impact of the glomerular architecture. It should be noted that in multivariate analysis, none of the Banff Classification scores remained associated with eGFR, while endothelial density did. Given that our study primarily focuses on most normal biopsies, we have opted to employ a composite endpoint that includes a decline in eGFR. Similar composite criteria are commonly used in transplantation and radical nephrectomy studies that analyze kidney prognosis [55–57]. Because of the stringent inclusion criteria, our cohort is relatively small, potentially explaining the absence of multivariate effects observed for several glomerular parameters. The relatively low number of events also limits the interpretation of the multivariate analysis. Future work could explore the temporal evolution of these parameters through repeated biopsies, evaluate the impact of therapeutic interventions or assess them in a pathological context with distorted glomeruli, such as antibody-mediated rejections. We did not train our model on mesangial matrix since it is assessed in the mesangial matrix score, and we have previously trained a model for evaluating the tuft [12]. The 2019 Banff Classification recommends the use of electron microscopy, especially for assessing cg1a and peritubular capillary basement

membrane multilayering [17]. The fact that we do not routinely perform electron microscopy in our centers deviates from international standards and constitutes a potential limitation that could potentially impact the diagnosis of antibody-mediated rejection.

Our study effectively automated the specific recognition, quantification and measurement of intraglomerular cells and capillaries of non-pathological glomeruli. Our findings suggest that the assessment of endothelial and parietal epithelial cells may hold promise as potential markers for predicting the risk of graft loss in kidney transplants.

SUPPLEMENTARY DATA

Supplementary data are available at *ckj* online.

FUNDING

None.

AUTHORS' CONTRIBUTIONS

I.F., E.M., J.-M.R. and M.L. were responsible for conception, analysis and interpretation of data. I.F. and M.L. drafted the article. D.C., G.T., S.A.F., L.M., J.-B.G., M.F.V., J.B. and M.L. were responsible for histological digitalization and/or analysis. Deep learning algorithms programming and evaluations were carried out by E.M., M.A. and M.P., and P.B. I.F., D.C., G.T., D.D., C.T. and J.B. helped with patient data acquisition and analysis. C.T. and J.-B.G. provided intellectual content of critical importance to the work described. All authors gave final approval of the version to be published.

DATA AVAILABILITY STATEMENT

The data underlying this article will be shared on reasonable request to the corresponding author. The Application cohort data and Test cohort predictions are available at: https://figshare.com/s/1c6471dca7d848eea467. The five deep learning weight files are available at: https://github.com/SkinetTeam/Skinet_glomerular_features.

CONFLICT OF INTEREST STATEMENT

None declared.

REFERENCES

1. Henderson LK, Nankivell BJ, Chapman JR. Surveillance protocol kidney transplant biopsies: their evolving role in clinical practice. *Am J Transplant* 2011;**11**:1570–5. https://doi.org/10.1111/j.1600-6143.2011.03677.x
2. Cosio FG, El Ters M, Cornell LD *et al*. Changing kidney allograft histology early posttransplant: prognostic implications of 1-year protocol biopsies. *Am J Transplant* 2016;**16**:194–203. https://doi.org/10.1111/ajt.13423
3. Lee O, Kim MJ, Lee JE *et al*. The protective role of protocol biopsy for allograft kidney maintenance in kidney transplantation. *Transplant Proc* 2023;**55**:756–68. https://doi.org/10.1016/j.transproceed.2023.01.029
4. Tanabe T. The value of long-term protocol biopsies after kidney transplantation. *Nephrology* 2014;**19**:2–5. https://doi.org/10.1111/nep.12253
5. Moreso F, Carrera M, Goma M *et al*. Early subclinical rejection as a risk factor for late chronic humoral rejection. *Transplantation* 2012;**93**:41–6. https://doi.org/10.1097/TP.0b013e31823bb647
6. Legendre C, Canaud G, Martinez F. Factors influencing long-term outcome after kidney transplantation. *Transpl Int* 2014;**27**:19–27. https://doi.org/10.1111/tri.12217
7. Loupy A, Mengel M, Haas M. Thirty years of the International Banff Classification for Allograft Pathology: the past, present, and future of kidney transplant diagnostics. *Kidney Int* 2022;**101**:678–91. https://doi.org/10.1016/j.kint.2021.11.028
8. Hara S. Banff 2013 update: pearls and pitfalls in transplant renal pathology. *Nephrology* 2015;**20**:2–8. https://doi.org/10.1111/nep.12474
9. Issa N, Lopez CL, Denic A *et al*. Kidney structural features from living donors predict graft failure in the recipient. *J Am Soc Nephrol* 2020;**31**:415–23. https://doi.org/10.1681/ASN.2019090964
10. Denic A, Bogojevic M, Subramani R *et al*. Changes in glomerular volume, sclerosis, and ischemia at 5 years after kidney transplantation: incidence and correlation with late graft failure. *J Am Soc Nephrol* 2023;**34**:346–58. https://doi.org/10.1681/ASN.2022040418
11. LeCun Y, Bengio Y, Hinton G. Deep learning. *Nature* 2015;**521**:436–44. https://doi.org/10.1038/nature14539
12. Marechal E, Jaugey A, Tarris G *et al*. Automatic evaluation of histological prognostic factors using two consecutive convolutional neural networks on kidney samples. *Clin J Am Soc Nephrol* 2022;**17**:260–70. https://doi.org/10.2215/CJN.07830621
13. Jaugey A, Maréchal E, Tarris G *et al*. Deep learning automation of MEST-C classification in IgA nephropathy. *Nephrol Dial Transplant* 2023;**38**:1741–51. https://doi.org/10.1093/ndt/gfad039
14. Zheng Z, Zhang X, Ding J *et al*. Deep learning-based artificial intelligence system for automatic assessment of glomerular pathological findings in lupus nephritis. *Diagnostics* 2021;**11**:1983. https://doi.org/10.3390/diagnostics11111983
15. Weis C-A, Bindzus JN, Voigt J *et al*. Assessment of glomerular morphological patterns by deep learning algorithms. *J Nephrol* 2022;**35**:417–27. https://doi.org/10.1007/s40620-021-01221-9
16. Govind D, Becker JU, Miecznikowski J *et al*. PodoSighter: a cloud-based tool for label-free podocyte detection in kidney whole-slide images. *J Am Soc Nephrol* 2021;**32**:2795–813. https://doi.org/10.1681/ASN.2021050630
17. Loupy A, Haas M, Roufosse C *et al*. The Banff 2019 Kidney Meeting report (I): updates on and clarification of criteria for T cell- and antibody-mediated rejection. *Am J Transplant* 2020;**20**:2318–31. https://doi.org/10.1111/ajt.15898
18. Tapiawala SN, Tinckam KJ, Cardella CJ *et al*. Delayed graft function and the risk for death with a functioning graft. *J Am Soc Nephrol* 2010;**21**:153–61. https://doi.org/10.1681/ASN.2009040412
19. Levey AS, Stevens LA, Schmid CH *et al*. A new equation to estimate glomerular filtration rate. *Ann Intern Med* 2009;**150**:604–12. https://doi.org/10.7326/0003-4819-150-9-200905050-00006
20. Jacq A, Tarris G, Jaugey A *et al*. Automated evaluation with deep learning of total interstitial inflammation and peritubular capillaritis on kidney biopsies. *Nephrol Dial Transplant* 2023;**38**:2786–98. https://doi.org/10.1093/ndt/gfad094

21. Cohen AH. Masson's trichrome stain in the evaluation of renal biopsies. An appraisal. *Am J Clin Pathol* 1976;**65**:631–43. https://doi.org/10.1093/ajcp/65.5.631
22. A Working Group of the International IgA Nephropathy Network and the Renal Pathology Society,Cattran DC, Coppo R *et al*. The Oxford classification of IgA nephropathy: rationale, clinicopathological correlations, and classification. *Kidney Int* 2009;**76**:534–45. https://doi.org/10.1038/ki.2009.243
23. Bajema IM, Wilhelmus S, Alpers CE *et al*. Revision of the International Society of Nephrology/Renal Pathology Society classification for lupus nephritis: clarification of definitions, and modified National Institutes of Health activity and chronicity indices. *Kidney Int* 2018;**93**:789–96. https://doi.org/10.1016/j.kint.2017.11.023
24. Cardinal H, Dieudé M, Hébert M-J. Endothelial dysfunction in kidney transplantation. *Front Immunol* 2018;**9**:1130. https://doi.org/10.3389/fimmu.2018.01130
25. Amabile N, Guérin AP, Leroyer A *et al*. Circulating endothelial microparticles are associated with vascular dysfunction in patients with end-stage renal failure. *J Am Soc Nephrol* 2005;**16**:3381–8. https://doi.org/10.1681/ASN.2005050535
26. Goligorsky MS. Pathogenesis of endothelial cell dysfunction in chronic kidney disease: a retrospective and what the future may hold. *Kidney Res Clin Pract* 2015;**34**:76–82. https://doi.org/10.1016/j.krcp.2015.05.003
27. Kocak H, Ceken K, Yavuz A *et al*. Effect of renal transplantation on endothelial function in haemodialysis patients. *Nephrol Dial Transplant* 2006;**21**:203–7. https://doi.org/10.1093/ndt/gfi119
28. Lamas S. Cellular mechanisms of vascular injury mediated by calcineurin inhibitors. *Kidney Int* 2005;**68**:898–907. https://doi.org/10.1111/j.1523-1755.2005.00472.x
29. Carman CV, Martinelli R. T lymphocyte-endothelial interactions: emerging understanding of trafficking and antigen-specific immunity. *Front Immunol* 2015;**6**:603. https://doi.org/10.3389/fimmu.2015.00603
30. Sis B, Jhangri GS, Bunnag S *et al*. Endothelial gene expression in kidney transplants with alloantibody indicates antibody-mediated damage despite lack of C4d staining. *Am J Transplant* 2009;**9**:2312–23. https://doi.org/10.1111/j.1600-6143.2009.02761.x
31. Mohandes S, Doke T, Hu H *et al*. Molecular pathways that drive diabetic kidney disease. *J Clin Invest* 2023;**133**:e165654. https://doi.org/10.1172/JCI165654
32. Salmon AHJ, Ferguson JK, Burford JL *et al*. Loss of the endothelial glycocalyx links albuminuria and vascular dysfunction. *J Am Soc Nephrol* 2012;**23**:1339–50. https://doi.org/10.1681/ASN.2012010017
33. Daehn I, Casalena G, Zhang T *et al*. Endothelial mitochondrial oxidative stress determines podocyte depletion in segmental glomerulosclerosis. *J Clin Invest* 2014;**124**:1608–21. https://doi.org/10.1172/JCI71195
34. Shankland SJ, Anders H-J, Romagnani P. Glomerular parietal epithelial cells in kidney physiology, pathology, and repair. *Curr Opin Nephrol Hypertens* 2013;**22**:302–9. https://doi.org/10.1097/MNH.0b013e32835fefd4
35. Bronstein R, Pace J, Gowthaman Y *et al*. Podocyte-parietal epithelial cell interdependence in glomerular development and disease. *J Am Soc Nephrol* 2023;**34**:737–50. https://doi.org/10.1681/ASN.0000000000000104
36. Ronconi E, Sagrinati C, Angelotti ML *et al*. Regeneration of glomerular podocytes by human renal progenitors. *J Am Soc Nephrol* 2009;**20**:322–32. https://doi.org/10.1681/ASN.2008070709
37. Appel D, Kershaw DB, Smeets B *et al*. Recruitment of podocytes from glomerular parietal epithelial cells. *J Am Soc Nephrol* 2009;**20**:333–43. https://doi.org/10.1681/ASN.2008070795
38. Chang AM, Ohse T, Krofft RD *et al*. Albumin-induced apoptosis of glomerular parietal epithelial cells is modulated by extracellular signal-regulated kinase 1/2. *Nephrol Dial Transplant* 2012;**27**:1330–43. https://doi.org/10.1093/ndt/gfr483
39. Smeets B, Kuppe C, Sicking E-M *et al*. Parietal epithelial cells participate in the formation of sclerotic lesions in focal segmental glomerulosclerosis. *J Am Soc Nephrol* 2011;**22**:1262–74. https://doi.org/10.1681/ASN.2010090970
40. Schlöndorff D, Banas B. The mesangial cell revisited: no cell is an island. *J Am Soc Nephrol* 2009;**20**:1179–87.
41. Avraham S, Korin B, Chung J-J *et al*. The mesangial cell—the glomerular stromal cell. *Nat Rev Nephrol* 2021;**17**:855–64. https://doi.org/10.1038/s41581-021-00474-8
42. Kim NH. Podocyte hypertrophy in diabetic nephropathy. *Nephrology (Carlton)* 2005;**10**:S14–6.
43. Rosenberg AZ, Kopp JB. Focal segmental glomerulosclerosis. *Clin J Am Soc Nephrol* 2017;**12**:502–17. https://doi.org/10.2215/CJN.05960616
44. Garg P. A review of podocyte biology. *Am J Nephrol* 2018;**47**:3–13. https://doi.org/10.1159/000481633
45. Yang Y, Hodgin JB, Afshinnia F *et al*. The two kidney to one kidney transition and transplant glomerulopathy: a podocyte perspective. *J Am Soc Nephrol* 2015;**26**:1450–65. https://doi.org/10.1681/ASN.2014030287
46. Menon R, Otto EA, Berthier CC *et al*. Glomerular endothelial cell-podocyte stresses and crosstalk in structurally normal kidney transplants. *Kidney Int* 2022;**101**:779–92. https://doi.org/10.1016/j.kint.2021.11.031
47. Agustian PA, Schiffer M, Gwinner W *et al*. Diminished met signaling in podocytes contributes to the development of podocytopenia in transplant glomerulopathy. *Am J Pathol* 2011;**178**:2007–19. https://doi.org/10.1016/j.ajpath.2011.01.042
48. Müller-Deile J, Bräsen JH, Pollheimer M *et al*. Graft growth and podocyte dedifferentiation in donor-recipient size mismatch kidney transplants. *Transplant Direct* 2017;**3**:e210. https://doi.org/10.1097/TXD.0000000000000728
49. Naik AS, Aqeel J, Wang SQ *et al*. Urine marker analysis identifies evidence for persistent glomerular podocyte injury across allograft lifespan. *Clin Transplant* 2021;**35**:e14457. https://doi.org/10.1111/ctr.14457
50. Schönenberger E, Ehrich JH, Haller H *et al*. The podocyte as a direct target of immunosuppressive agents. *Nephrol Dial Transplant* 2011;**26**:18–24. https://doi.org/10.1093/ndt/gfq617
51. Vivarelli M, Massella L, Ruggiero B *et al*. Minimal change disease. *Clin J Am Soc Nephrol* 2017;**12**:332–45. https://doi.org/10.2215/CJN.05000516
52. Naik AS, Afshinnia F, Cibrik D *et al*. Quantitative podocyte parameters predict human native kidney and allograft half-lives. *JCI insight* 2016;**1**:e86943. https://doi.org/10.1172/jci.insight.86943
53. Naik AS, Afshinnia F, Aqeel J *et al*. Accelerated podocyte detachment early after kidney transplantation is related to long-term allograft loss of function. *Nephrol Dial Transplant* 2019;**34**:1232–9. https://doi.org/10.1093/ndt/gfy350
54. Doreille A, Azzi F, Larivière-Beaudoin S *et al*. Acute kidney injury, microvascular rarefaction, and estimated glomerular filtration rate in kidney transplant recipients. *Clin J Am Soc Nephrol* 2021;**16**:415–26. https://doi.org/10.2215/CJN.07270520

55. Coresh J, Turin TC, Matsushita K *et al.* Decline in estimated glomerular filtration rate and subsequent risk of end-stage renal disease and mortality. *JAMA* 2014;**311**:2518–31. https://doi.org/10.1001/jama.2014.6634
56. Clayton PA, Lim WH, Wong G *et al.* Relationship between eGFR decline and hard outcomes after kidney transplants. *J Am Soc Nephrol* 2016;**27**:3440–6. https://doi.org/10.1681/ASN.2015050524
57. Denic A, Gaddam M, Moustafa A *et al.* Tubular and glomerular size by cortex depth as predictor of progressive CKD after radical nephrectomy for tumor. *J Am Soc Nephrol* 2023;**34**:1535–45. https://doi.org/10.1681/ASN.0000000000000180

Received: 31.10.2023; Editorial decision: 15.12.2023